

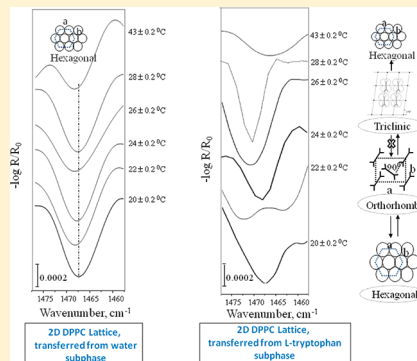
Unraveling Tryptophan Modulated 2D DPPC Lattices: An Approach toward Stimuli Responsiveness of the Pulmonary Surfactant

Nirod Kumar Sarangi and Archita Patnaik*

Department of Chemistry, Indian Institute of Technology Madras, Chennai 600 036, India

S Supporting Information

ABSTRACT: A molecular understanding on the preferential and selective interactions of L-tryptophan, a major component of surfactant proteins, with 1,2-dipalmitoyl-sn-glycero-3-phosphocholine (DPPC) is important in the metabolic cycle of the pulmonary surfactant. In view of this, interfacial signals of interest in real time were tapped with aligned DPPC monolayers over a physiological tryptophan subphase using extremely surface sensitive 2D vibrational spectroscopy. Polarization-modulated and angle dependent Fourier transform infrared reflection absorption spectroscopy (FT-IRRAS) of DPPC monolayers on water and L-tryptophan subphases depicted fine structure/conformation differences in the interaction modes, evidenced from changes in the vibrational band intensities and frequencies under conditions of controlled 2D surface pressure. The computed 1:1 adducts of DPPC/H₂O and DPPC/tryptophan in support of FT-IRRAS fine structure characteristics demonstrated binding in interfacial DPPC-tryptophan adducts to be driven by cation-π interactions alongside hydrogen bonding of carbonyl and phosphate groups of the lipid with NH₃⁺ of the zwitterionic tryptophan. In situ spectroscopy enabled assignment of relative orientations of the equivalent -CH₂ functional groups from the polarized XY plane transition moments with component intensities of the split orthorhombic CH₂ mode. A larger molecular tilt of 37° for the DPPC monolayer over tryptophan subphase in comparison with that over water (26°) substantiated the DPPC headgroup interaction with tryptophan, complemented through δ (N^{+(CH₃)₃), ν_{as} (PO₂⁻), ν_s (PO₂⁻), ν_{as} (C-N⁺⁻C), and ν (C=O) vibrational features. The IRRAS spectral features of the DPPC 2D condensed phase showed distinct tryptophan-induced temperature dependent lattice phase transitions: hexagonal → orthorhombic → triclinic → hexagonal packing of the hydrocarbon chains was noted over a subphase temperature range from 20 to 43 °C. The temperature dependent 2D DPPC lattice characteristics cited in this work will aid in understanding the impact of a temperature pulse toward the membrane functionality.}



INTRODUCTION

The physicochemical properties of biological membranes are of critical importance for understanding specific membrane functions.¹ The structural changes that the multicomponent biological membranes undergo in physiological conditions help define characteristic membrane functions. Incorporation of proteins into lipid bilayers influences the membrane phase behavior, thereby affecting membrane dynamics and modifying its biological functions. Aromatic amino acids as constituents of membrane proteins and peptides have played important roles in directed interactions between proteins and lipids in the region of polar head groups.^{2–4} Tryptophan has both hydrophobic (indole N–H) and hydrophilic (zwitter-ionic segment) character; consequently, it partitions at the hydrophobic–hydrophilic interfaces in lipid bilayers.^{5,6} The physical basis for the preference of tryptophan and tyrosine residues is widely believed to arise from amphiphatic interactions related to hydrogen bonding and/or dipole interactions.⁷

Unraveling dynamical processes of transport phenomena, energy transfer, molecular interactions, as well as chemical reactions in a 2D perspective is a great challenge. Keeping in mind the molecular structure determination, the air–water (A/W) interface permits facile control of many experimental parameters,

such as, temperature, phase state, molecular packing and orientation, lateral pressure, surface viscosity, subphase composition, and domain size and shape with full understanding of superstructure/orientation of the film-forming molecules/aggregates. In this regard, Fourier transform infrared reflection absorption spectroscopy^{8–21} (FT-IRRAS), X-ray and neutron techniques,^{22–24} and Brewster angle microscopy (BAM)^{25,26} have been extensively used.

Polymorphism in phospholipid monolayers investigated by Albrecht et al.²⁷ from pressure–area isotherms and area–temperature isobars has provided an understanding of the first-order transition between the expanded (fluid) and the condensed (crystalline) states of the films. The transition between two crystalline states was ascribed to be of weak first order with transition enthalpy ∼−10 J/mol. For π > 15 dyn/cm, the polymorphic states of the phospholipid monolayers observed at decreasing areas were characterized as fluid isotropic (I) (hydrocarbon chains normal to water surface), fluid anisotropic (II)

Received: August 15, 2011

Revised: October 9, 2011

Published: October 14, 2011

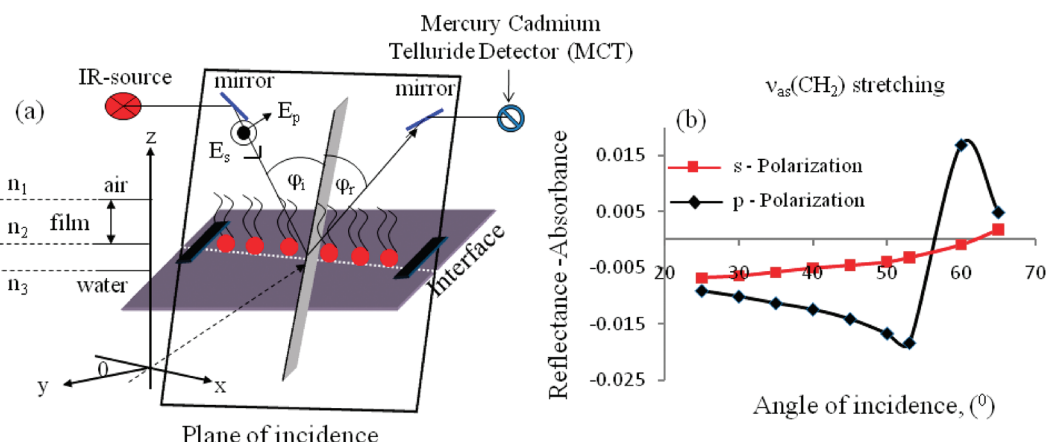


Figure 1. (a) Optical set up of the in situ polarization modulated FT-IRRAS arrangement illustrating the three phase optical coordinates. The Bruker XA 511 reflection attachment with the shuttle trough is merged with the main trough with the oriented monolayers. (b) Polarization dependent Brewster angle concept at the three phase (air ($n_1 = 1$), film (n_2), and water ($n_3 = 1.33$)) interface with reflectance-absorbance from the monolayers. Brewster angle was estimated as $\tan^{-1}(n_3/n_1) = \tan^{-1}(1.33/1.0) = 54.5^\circ$.

(tilted chains), tilted crystalline (III), and nontilted crystalline (IV) phases. A relation between monolayer to bilayer phase transition was established; for L- α -dipalmitoyllecithin, monolayers at an external pressure of 12.5 dyn/cm corresponded to bilayers at maximum hydration. Effect of divalent cations on a zwitter-ionic phospholipid monolayer through in situ X-ray scattering revealed lowering of surface pressure for the fluid (LE) to condensed (L2) phase transition in a strongly ion-specific manner. The two-dimensional lattice dimensions and the tilt of the lipid's alkyl tails in the L2 phase depended solely on the excess surface pressure above the transition pressure and not on the cation present.²⁸ A molecular theory was developed by Grillo et al.²⁹ to assess the effect of adsorption of a macro-ion onto a 1,2-dipalmitoyl-sn-glycero-3-phosphocholine (DPPC) bilayer on its phase behavior. Taking charge density, size, and molecular conformation into account, the favorable electrostatic interactions between the negatively charged macro-ion and the zwitterionic phosphocholine head-groups led to stabilization of the DPPC bilayer gel phase with increase in the main chain transition temperature. Gzyl-Malcher et al.³⁰ discussed interactions of mixed monolayers of DPPC and DPTAP (dipalmitoyl trimethyl ammonium propane) with the phytohormone, indolilo-3-acetic acid, and selenate anions in the aqueous subphase. A pronounced condensing effect for the binary monolayers were related with reorientation of the P⁻-N⁺ dipole of the DPPC headgroup from a parallel to a more vertical orientation. A recent report indicated TiO₂ nanoparticles to have altered the structure and function of a pulmonary surfactant.³¹ Particle size and surface area respectively played a critical role for the surfactant response in the lung. In spite of the above DPPC interfacial interactions, insight on its 2D lattice structure under varied experimental conditions is clearly missing.

In the present investigation, selective interaction of L-tryptophan as a major component of surfactant proteins with the model lipid DPPC membrane was mooted in a physiologically relevant tryptophan concentration range in the absence of competing factors of protein conformation and membrane perturbation. The first aim was to investigate the phase behavior and acyl chain orientation in DPPC monolayers and their 2D lattices upon changes in the membrane environment as a function of temperature and pressure adopting surface manometry and angle dependent real time polarized FT-IRRAS. The second objective

was to analyze the effect upon incorporating zwitterionic tryptophan in the subphase and investigate the interfacial lipid/amino acid interaction from (a) the nature of the polar headgroup and acyl chains of the phospholipid and (b) the evolution of 2D lattice structure and packing as a function of temperature and interfacial composition. The observations indicated electrostatic interactions and hydrophobicity as important factors in determining the optimal structure of lipid monolayers, substantiated from density functional theory (DFT) computations. The unique and notable findings from this study reflected on temperature dependent hexagonal to orthorhombic reversible 2D crystal phase transition, followed by an irreversible triclinic phase at a higher temperature, and ultimately reverting back to the hexagonal subcell structure at a maximum temperature of 43 °C.

EXPERIMENTAL SECTION

Materials and Methods. DPPC of 99% purity was obtained from Sigma (St. Louis, MO) and L-tryptophan (99% purity) from Merck (SSEA, Mumbai) and were used as received. Spreading solutions were prepared from chloroform (HPLC grade, Uvasol, Merck India Ltd.) for the formation of interfacial Langmuir monolayers. Temperature dependent experiments at 43 °C were initiated in reference to the tricritical point in lipid monolayers for the separation of the LE and LC phases.¹³ The pressure-area isotherms were acquired from an R&K Langmuir mini-trough (Germany) of total area 184 cm² with hydrophilic Delrin barriers for the compression-expansion of the monolayers. Ultrapure water of resistivity 18.2 MΩ cm was used as the subphase for all monolayer studies produced by a two stage Elix-3 and Milli-Q (Millipore Academic) system. The water subphase was modified with 0.001–0.05 mg/mL L-tryptophan (1–5 wt %) for recording the structural features of DPPC-L-tryptophan interaction using s and p polarized FT-IRRAS spectroscopy.

In Situ FT-IRRAS Experimental Set Up. Figure 1 illustrates the details of the polarized FT-IRRAS instrumentation. Measurements were performed on a Brueker Optic GmbH (Germany) Vertex 70 spectrometer equipped with a Mercury – Cadmium Telluride (MCT) detector (spectral resolution 0.1 cm⁻¹) and a home-built optical attachment placed on a vibration isolated

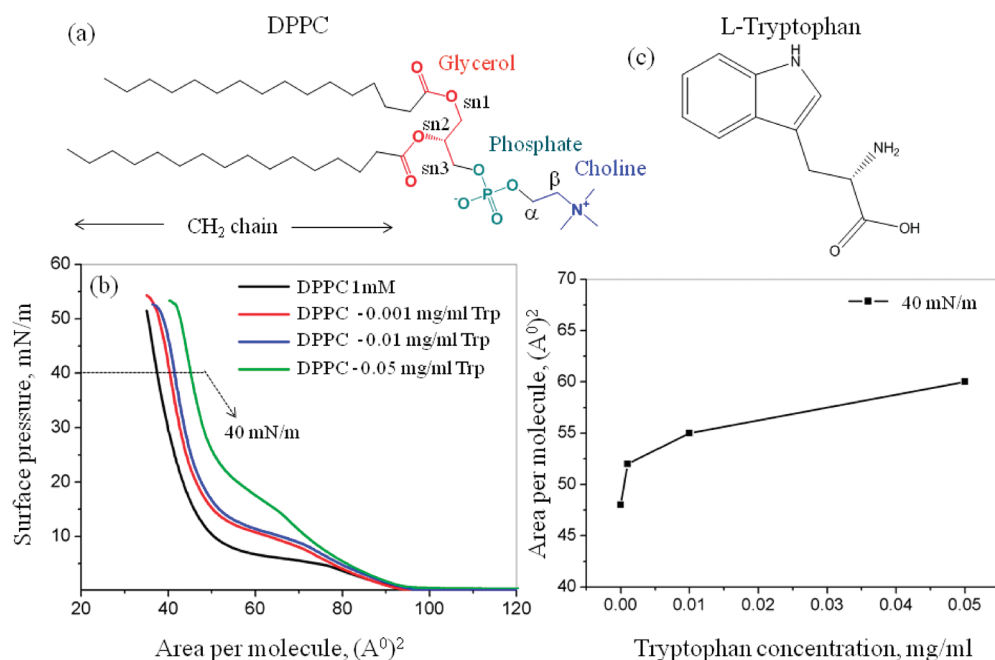


Figure 2. (a) Chemical structures of DPPC and L-tryptophan (Trp). (b) Pressure–area isotherms of DPPC monolayers over water and tryptophan subphases. (c) Variation of monolayer area of the condensed phase at 40 mN/m as a function of subphase tryptophan concentration.

Newport I-2000 table (Fountain Valley, CA). The spectrometer was equipped with an external variable-angle reflectance accessory XA 511 coupled to a custom-designed Langmuir trough R&K (Germany). The IR beam was focused onto the water surface with an off-axis parabolic mirror with a focal length of 120 mm and the desired angle of incidence was obtained when the computer driven stepper motors rotated the mirrors. The angle of incidence was varied between $(25\text{--}65)\pm1^\circ$ from the surface normal, the latter being the maximum grazing incidence obtainable. Alternate s and p-polarized spectra were acquired with a resolution of 4 cm^{-1} by coaddition of 2048 (for s-polarization) and 4096 (for p-polarization) scans. The entire experimental setup was enclosed and purged with dry N_2 . Figure 1a depicts E_s and E_p as the electric field vectors for s- and p-polarization with φ_i and φ_r , as the angles of incidence and reflection, respectively. In Figure 1b, the variation of reflectance-absorbance (RA) for the methylene (CH_2) antisymmetric stretching vibration as a function of angle of incidence is illustrated, where, RA is defined as $-\log R/R_0$, with R and R_0 as the reflectivities of the DPPC monolayer covered and bare water subphase respectively. This experimental finding suggests the concept of Brewster angle, where the intensity of the IRRAS band becomes negative when the reflectivity of the film covered surface exceeds that of the bare water surface. For p-polarization of the IR beam with incident angles smaller than the Brewster angle, the phase change of light upon reflection is $\sim 0^\circ$, whereas at the Brewster angle is close to 54.5° . Spectral acquisitions were done at the desired isobaric pressures at $22\text{ }^\circ\text{C}$ and pH 6.4. A 4 cm^{-1} spectral resolution demanded a 10 min recording time for each spectrum. The IRRAS spectra were defined with wavenumber peak positions to better than $\pm 0.01\text{ cm}^{-1}$ precision and the observed scatter were thus due to inherent data fluctuations in the monolayers.

Computational Details. Geometry optimization of the individual molecules of interest and the 1:1 adducts was done using

density functional calculations at a B3LYP/6-31G (d, p) level of theory as included in Gaussian 03 set of programs.³²

RESULTS AND DISCUSSION

Figure 1a depicts the chemical structures of DPPC and L-tryptophan. The amphiphilic nature of DPPC allows it to orient and organize at the air–water interface as an ordered monolayer assembly and to undergo various phase transformations as a function of surface pressure.³³ The conformational space of a single tryptophan in water was studied by different NMR techniques, and the major gauche (g^-) conformation with the indole ring in an orientation perpendicular to the $C^\alpha\text{--}C^\beta$ bond was calculated to contain about 70% of all conformations in a zwitterionic form.^{34,35} Accordingly, the optimized zwitterionic structure of tryptophan is shown in Figure S1(b) in the Supporting Information (SI) with the molecular coordinates whose transition dipole moment vectors remain in the plane of the indole ring. The surface pressure–area ($\pi\text{--}A$) isotherms of pure DPPC monolayers over water as well as tryptophan subphases at $22\text{ }^\circ\text{C}$ as a function of tryptophan concentration are depicted in Figure 2b. The isotherm characteristic of DPPC reveals typical 2D phase states during monolayer compression.³⁶ Modeling the DPPC headgroup as a rectangle, the estimated area, $6.64 \times 7.30 = 48.2\text{ \AA}^2$ from DFT B3LYP/6-31G (d, p) geometry optimized structures (Figure S1(a), SI) complies with the experimental monolayer area obtained from manometry in Figure 2b. The $\pi\text{--}A$ isotherms of the DPPC monolayers bear a slight variation in lift-off areas as 89.1 and 92.4 \AA^2 for water and tryptophan subphases, respectively, implying the absence of a two component (DPPC–L-tryptophan) monolayer. The typical plateau, located at 5 mN/m indicates the coexistence of LE and LC phases relative to the pure DPPC. Whereas, a smaller area per lipid corresponds to greater steric and electrostatic repulsions between the head-groups due to more parallel dipoles, the higher

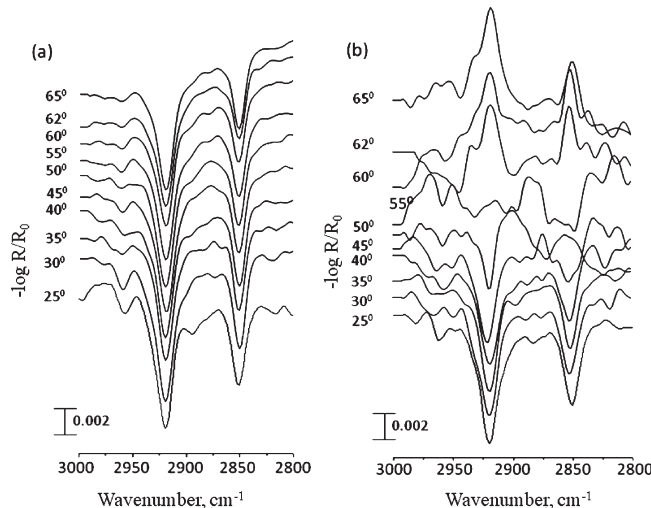


Figure 3. FT-IRRAS spectra of methylene stretching region of DPPC monolayers on tryptophan subphase for (a) s-polarized and (b) p-polarized radiation at varied angles of incidence.

area per lipid, corresponding to the liquid-crystalline phase, arises from an increase in the conformational freedom of the lipid chains. Increasing the amount of tryptophan clearly modified the shape and location of the curves, shifting the LE–LC plateau toward higher areas; in particular, the curves relative to the tryptophan added monolayers showed the apparent plateau at larger areas and larger surface pressures. However, no distinct tryptophan-rich domain was observed from the monolayers, confirmed from the absence of N–H stretching bands in the IRRAS spectra, discussed in the following sections. In Figure 2c, a gradual increase in the weight percentage of subphase tryptophan resulted in a nominal increase in the mean molecular areas over that of pure DPPC monolayers. It is apparent that the collapse pressures of the tryptophan modulated films for its lower content lie between the collapse pressures of the pure DPPC and the higher tryptophan containing films, indicating a certain degree of molecular interaction between the two components, exemplified from molecular modeling and spectroscopy in the following sections.

Real Time FT-IRRAS Spectroscopic Investigation of DPPC–Tryptophan Interfacial Structures. The interfacial DPPC monolayers with a polar headgroup consisting of a positively charged quaternary ammonium group, a negatively charged phosphate moiety, and an intermediate glycerol unit with two hydrophobic chains attached by ester linkages were studied with FT-IRRAS spectroscopy to analyze the monolayer structure, its degree of hydration and interaction with the polar head groups of zwitterionic L-tryptophan. In the following sections, a careful analysis of the polar headgroup region from the C=O stretching mode of the ester group, CH bending and CN stretching modes in the choline moiety and antisymmetric and symmetric phosphate stretching bands of the phosphodiester is presented. Adopting Gaussian deconvolution, the real time angle dependent and polarization induced spectral differences indicated fine structural differences between the DPPC monolayers over water and tryptophan subphases from which characteristic molecular tilt angles and 2D lattices of DPPC were established.

In Figure 3, panels a and b, angle dependent FT-IRRAS spectra over tryptophan subphase illustrate the characteristic ν_a and

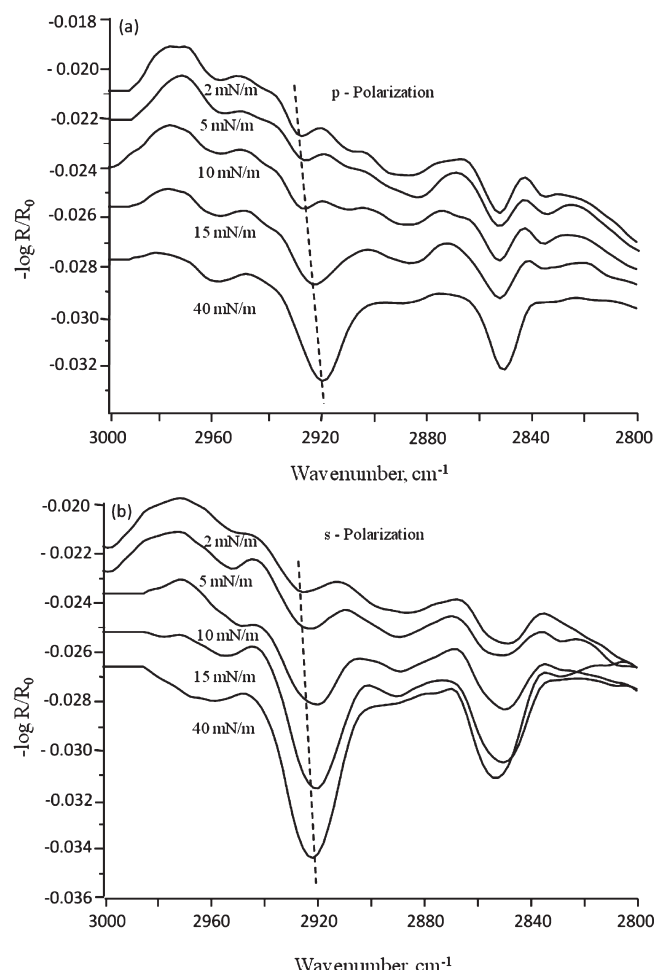


Figure 4. Methylene ν_a and ν_s stretching modes of DPPC monolayer on tryptophan subphase at varied surface pressures for (a) p- and (b) s-polarized IR beams at 22 °C and 40° angle of incidence.

$\nu_s(\text{CH}_2)$ stretching modes for s- and p-polarized beams, respectively. The hydrophobic hydrocarbon chains were analyzed from the conformation sensitive CH_2 stretching and bending vibrational modes. For preferential orientation of CCC plane of the hydrocarbon chains,²⁰ the s-polarized IRRAS spectra were not as sensitive as the p-polarized ones. However, the intensity ratio remained almost unchanged at 0.15, independent of the angle of incidence for p- and s-polarizations, but with a fluctuation near the Brewster angle for p-polarization (cf. Figure S2, SI). These characteristics indicated the hydrocarbon chains in the monolayers to be uniaxially oriented with respect to surface normal. Membrane lipid perturbation by tryptophan in the subphase could have arisen either from the acyl chain interfacial region or from the polar headgroup. However, most studies on the physical state of the membrane have been carried out using the C–H asymmetric and symmetric stretching bands.³⁷

The temperature dependent intensity ratios (cf. Figure S3, SI) for DPPC monolayers gave clear explanation where tryptophan induced a broad LE–LC phase transition. Figure 4, panels a and b, depicts prominent frequency shifts of ~ 8 and 3 cm^{-1} for ν_a (CH_2) and ν_s (CH_2) stretching vibrations, respectively, at increasing π , implying a deviation in the direction of the transition dipole moment. A conversion from gauche conformed alkyl chains at lower π to an all-trans conformation

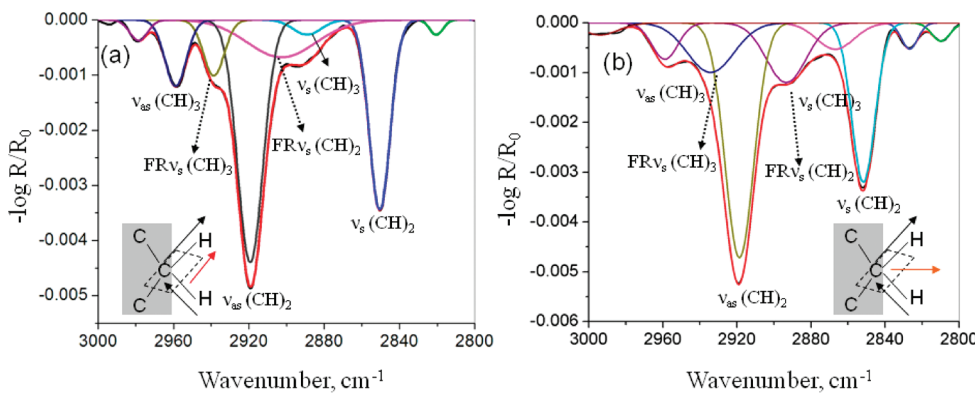


Figure 5. p-Polarized FT-IRRAS Gaussian deconvoluted spectra in CH_2 stretching mode region of DPPC monolayers on (a) water and (b) on tryptophan subphases at an equilibrium surface pressure of 40 mN/m at 22 $^{\circ}\text{C}$. Insets depict the directions of ν_{as} and ν_s transition dipole moments for both systems.

(near-perpendicular to the water surface) at higher π condensed phase has thus resulted.

The spectral data confirm the ordered all-trans conformation maintained over the wide range of LC to the condensed phase region.

DPPC Hydrocarbon Tail Structure Driven by Tryptophan Induced Head Group Interaction. The direction of the transition dipole moments for methylene units are perpendicular to the alkyl chains with the $\nu_s(\text{CH}_2)$ transition moment oriented along the bisector of the methylene H—C—H bond angle, while the $\nu_{as}(\text{CH}_2)$ transition moment lies perpendicular to this. Insets of Figure 5, panels b and a, illustrate the phenomena respectively. Accordingly, for p-polarization, the methylene stretching band intensity was maximum, when all transition moments oriented horizontally, meaning, the hydrophobic chains were almost perpendicular to the water surface. On the water subphase in Figure 5a, the $\nu_{as}(\text{CH}_2)$ located at 2919 cm^{-1} and $\nu_s(\text{CH}_2)$ at 2850 cm^{-1} indicated an all-trans conformation of the alkyl chains. The $\nu_s(\text{CH}_3:\text{CH}_2)$ intensity ratio remained low, complying with the literature.³⁸

On the tryptophan subphase (Figure 5b), the $\nu_{as}(\text{CH}_2)$ at 2918 cm^{-1} and $\nu_s(\text{CH}_2)$ at 2851 cm^{-1} showed a slight increase in the fwhm values as compared to those over the water subphase. A significant shift in the terminal $\nu_s(\text{CH}_3)$ and $\nu_{as}(\text{CH}_3)$ vibrations along with the FR $\nu(\text{CH}_3)$ arose as a result of coupling of the fundamental vibration with an overtone³⁹ keeping the all-trans conformation of the methylene chains for both water and tryptophan subphases. The p-polarization dependent peak assignments along with the fwhm and integrated percentage areas for each vibration are tabulated for DPPC/trypophan in Table S1, SI.

Structural Investigation of Polar Head Group Regions [$\text{N}^+(\text{CH}_3)_3$, $\text{C}-\text{N}^+-\text{C}$, and PO_2^-] of DPPC Monolayers over Water and Tryptophan Subphases. Membrane lipid perturbations by peripheral membrane proteins and soluble proteins have been invariably found associated to membranes.²² According to the present FT-IRRAS spectral results, the interaction occurred at many levels of the bilayer structure. The phosphate region of the IRRAS spectra revealed hydrogen bond formation by the electrostatic replacement of the charged polar headgroup with tryptophan. The CH_3 bending mode of the choline moiety and the phosphate group of DPPC are sensitive to Coulombic interactions and hydrogen bonding respectively. The spectra in Figure 6, panels a and b, show important absorption features

originating from the polar DPPC headgroup, namely, the asymmetric CH_3 bending and the bending $\text{N}^+(\text{CH}_3)_3$ vibrational modes with E and A_1 symmetry from the choline moiety. The dipole moment vector for the E symmetry mode of the choline group⁴⁰ is oriented perpendicularly to the CN bond (cf. inset Figure 6a), whereas that for the A_1 symmetry lies along the C_{3v} axis in the direction of CN bond in the inset of Figure 6b. Thus, the two $\delta(\text{N}^+(\text{CH}_3)_3)$ absorption bands belonging to E and A_1 symmetries are centered at 1475 and 1496 cm^{-1} for water and at 1480 and 1495 cm^{-1} for tryptophan subphase, corresponding to out of phase degenerative bending and in-phase symmetric bending modes, respectively. Since the choline portion of the headgroup will not form a hydrogen bond³⁷ with H_2O , a difference of $\sim 5 \text{ cm}^{-1}$ for E symmetry (cf. Table 1) indicates the environment of choline moiety to have been affected by tryptophan through cation- π and electrostatic interactions.

Table 1 shows distinct variations in the choline $\delta(\text{N}^+(\text{CH}_3)_3)$ vibrational frequencies for DPPC monolayers over water and tryptophan subphases. Earlier theoretical simulations have provided additional insight into the DPPC/water interfacial structure, where the water molecules were able to penetrate up to the carbonyl groups of the lipid tails.⁴¹ In Figure 6, panels c and d, a detailed analysis of the CN stretching modes provides information on the conformation of the choline moiety for tryptophan and water subphases respectively. In the former case, the CN ν_{as} and ν_s stretching (trans) bands are located at 970/978 and 950 cm^{-1} , respectively, with the lower wavenumber $\sim 917 \text{ cm}^{-1}$ band originating from the ν_s stretching (gauche) mode (cf. Table 1). The number and position of these modes are dependent on the conformation, trans or gauche, of O—C—C—N of the choline moiety.²⁵ The p-polarized ν_{as} stretching vibration showed the emergence of a new feature only over the tryptophan subphase at a higher frequency 978 cm^{-1} with a 15 wt % contribution to the overall choline group vibrations. It is to be noted here that this higher frequency feature was absent in the p-polarized spectrum acquired from the water subphase, confirming substantial contribution from the cation (choline N^+)— π (indole ring/trypophan) type interaction at a tryptophan rich interface. Here, the electrical vector of the p-polarized radiation remained in-phase with the delocalized charge cloud of tryptophan yielding finite peak intensity.

The phosphate asymmetric stretching mode $\nu_{as}(\text{PO}_2^-)$ for the water subphase in Figure 7a splits into three absorptions

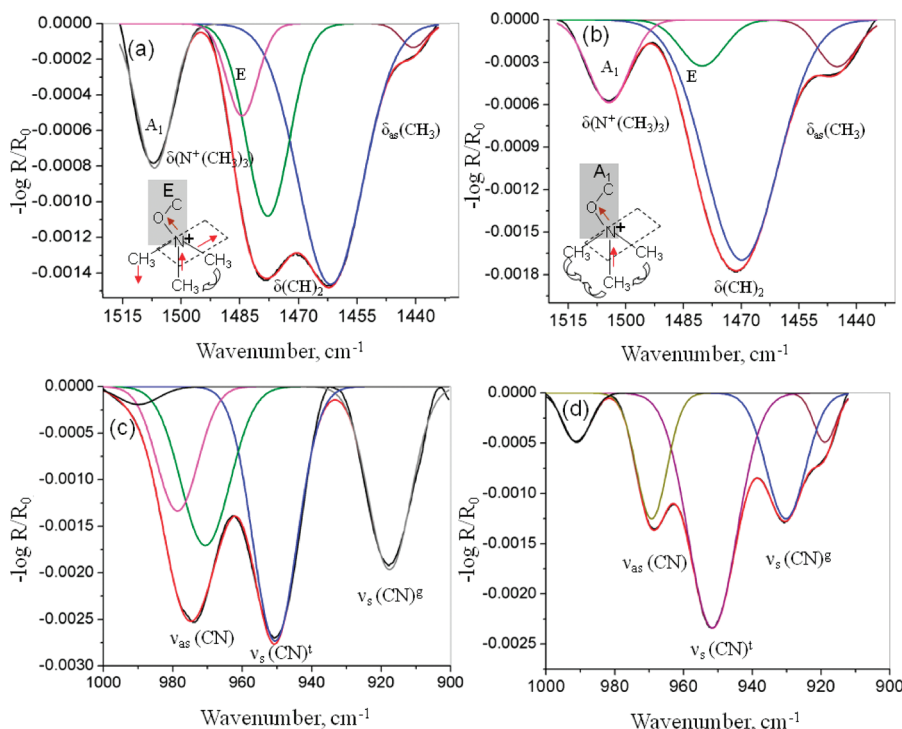


Figure 6. p-Polarized FT-IRRAS Gaussian deconvoluted spectra for $\delta(\text{N}^+(\text{CH}_3)_3)$, $\delta(\text{CH}_2)$, $\delta_{\text{as}}(\text{CH}_3)$, and ($\text{C}-\text{N}^+-\text{C}$) stretching mode regions of DPPC monolayers over tryptophan (a and c) and water (b and d) subphases at 40° angle of incidence at a surface pressure 40 mN/m. Insets depict the directions of the transition dipole moments for E and A_1 symmetry.

Table 1. p-Polarized Choline Vibrational Frequencies of DPPC Monolayers over Water and Tryptophan Subphases

fundamental vibrations	peak position/cm ⁻¹ (tryptophan)	fwhm (cm ⁻¹)	area %	peak position/cm ⁻¹ (water)	fwhm (cm ⁻¹)	area %
$\delta(\text{N}^+(\text{CH}_3)_3)$ A_1	1495	10.77	14.73	1496	12.53	13.62
E	1480	9.48	8.47	1475	13.23	8.06
$\delta(\text{CH}_2)$	1473/1465	13.28/19.84	24.8/50.03	1469	22.39	71.97
$\delta_{\text{as}}(\text{CH}_3)$	1445	7.69	1.73	1448	11.86	7.33
$\nu_{\text{as}}(\text{C}-\text{N}^+-\text{C})$	970.62	16.66	23.86	970.85	16.66	38.53
	978.65	13.94	15.67			
$\nu_{\text{s}}(\text{C}-\text{N}^+-\text{C})^t$	950.59	15.06	34.65	945.13	15.77	42.26
$\nu_{\text{as}}(\text{C}-\text{N}^+-\text{C})^g$	917.62	14.33	23.66	920.10	7.95	3.78

where the maxima are located at 1233, 1246, and 1285 cm⁻¹. The band at 1233 cm⁻¹ corresponds to a well hydrated, evenly hydrogen bonded phosphate group (fwhm = 27.5 cm⁻¹). The 1246 cm⁻¹ feature with fwhm 27.5 cm⁻¹ corresponds to a strongly hydrated phosphate group, and that at 1285 cm⁻¹ with very low absorbance arises due to the dry phosphate group.⁴³ The absence of this feature for the tryptophan subphase in Figure 7b implies the presence of the H-bonded phosphate group in the tryptophan environment (cf. Table 2). Further, the phosphate asymmetric stretching mode $\nu_{\text{as}}(\text{PO}_2^-)$ for the tryptophan subphase is split into two important absorptions with maxima located at 1223 and 1245 cm⁻¹. The band centered at 1223 cm⁻¹ confirms a stronger hydrogen bond interaction between the phosphate and tryptophan as compared to that in water at 1233 cm⁻¹. The wide range (1200–1300 cm⁻¹) of absorptions in the asymmetric phosphate stretching region indicates that the phosphate group in DPPC has different degrees of hydration.

The high frequency band corresponds to the weekly hydrated phosphate group, while the low frequency band is indicative of a well hydrated, evenly hydrogen bonded phosphate group. A detail analysis of the deconvoluted peaks shows significant changes in the $\nu_{\text{as}}(\text{PO}_2^-)$ modes upon switching from water to the tryptophan subphase. Similarly, the $\nu_{\text{s}}(\text{PO}_2^-)$ bands centered at 1088 and 1083 cm⁻¹ were observed for water and tryptophan subphases, respectively. The bands shifting to lower wavenumbers for the DPPC–tryptophan interaction could be attributed to tryptophan's ability to enhance the second ionization state of the phosphate group at the physiological condition.⁴⁴ The insets of Figure 7 show the transition dipole moment of the symmetric phosphate stretching mode to lie along the bisector of the phosphate nonesterified group and the asymmetric stretching mode in the same plane, making a normal angle to the direction of the dipole moment of the symmetric stretching mode. At the air/water interface, the phosphate group retains its tetrahedral symmetry, where the esterified line of the phosphate group

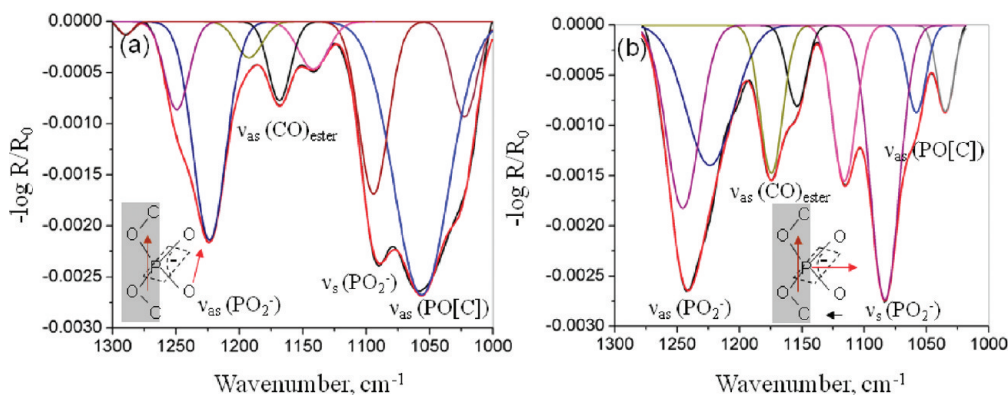


Figure 7. p-Polarized Gaussian deconvoluted FT-IRRAS spectra in the phosphate group stretching mode region of DPPC monolayers on (a) water and (b) tryptophan subphase. Insets show marked directions of the transition dipole moments of the asymmetric and symmetric phosphate stretching modes and their relation to the OPO line of the esterified phosphate group.

Table 2. p-Polarized Phosphate Vibrational Frequencies of DPPC Monolayers over Water and Tryptophan Subphases

fundamental vibrations	peak position/cm ⁻¹ (tryptophan)	fwhm (cm ⁻¹)	area %	peak position/cm ⁻¹ (water)	fwhm (cm ⁻¹)	area %
$\nu_{as}(\text{PO}_2^-)$	1223.71	44.71	20.71	1233.29	27.49	10.73
	1245.48	30.63	18.53	1246.09	27.17	9.08
$\nu_s(\text{PO}_2^-)$	1083.49	26.87	24.43	1088.80	23.74	10.09
$\nu_{as}(\text{PO}[\text{C}])$	1034.97	15.61	4.48	1037.42	17.57	8.79
$\nu_{as}(\text{CO})_{\text{ester}}$	1174.84	21.28	10.42	1186.07	27.52	8.90

[C]OPO[C] line is normal to the directions of both asymmetric and symmetric dipole moments. The corresponding $\nu_{as}(\text{PO}[\text{C}])$ band was centered at 1037 cm⁻¹ with a fwhm of 17.57 cm⁻¹ for the water subphase, and a decrease in frequency for the same was observed around 1035 cm⁻¹ (fwhm = 15.61 cm⁻¹) for the tryptophan subphase. Similarly the $\nu_{as}(\text{CO})_{\text{ester}}$ band at 1186 cm⁻¹ for the water subphase shifted to 1174 cm⁻¹ for the tryptophan subphase (cf. Table 2). A theoretical study of the PO₂⁻ moiety of methylphosphocholine showed loss of electron density of the P=O bonds upon hydration and was attributed to its strong hyperconjugation with the water O—H antibonding orbital, resulting in weakened P=O bonds and a red shift.⁴⁵

The binding of tryptophan through hydrogen bonding as well as electrostatic interaction creates a hydrophobic environment around the DPPC headgroup, which is an important factor for understanding interfacial behavior of biomembranes.⁴⁶ It is therefore interesting to speculate the binding to be sufficient to displace some of the water molecules near the lipid environment, explained by water-squeeze-out mechanism.⁴⁷

Effect of Tryptophan on C=O Vibrations of Interfacial DPPC Monolayers. The effects of tryptophan may result from differential interactions at the interfacial region of the DPPC membrane, where the carbonyl group is situated at the interface between the hydrophobic hydrocarbon chains and the more hydrophilic headgroup region. The p-polarized $\nu(\text{C=O})$ band of the DPPC monolayer in Figure 8, panels a and b, splits into at least two bands: the upfield peak due to the non-hydrogen bonded C=O group and the downfield peak due to the hydrogen bonded C=O group, centered at 1733 and 1714 cm⁻¹ with fwhm 12.64 cm⁻¹, respectively, for the tryptophan subphase in reference to water subphase at 1741 and 1722 cm⁻¹ with fwhm

15.04 cm⁻¹ (cf. Table S2, SI). The much lower fwhm associated with the hydrogen bonded vibrational band implies a localized H-bonding of the type C=O···H₃N⁺ (area weight = 12%) for the tryptophan subphase, as compared to the predominant H-bonding existing over water subphase (area weight = 26%) in a more hydrated environment.

The position and width of the $\nu(\text{C=O})$ vibrations for the DPPC monolayers are thus dependent on the hydration environment of the ester moiety.⁴⁸ The red shift along with band narrowing from a tryptophan subphase are a cumulative effect of carbonyl-cation (NH₃⁺), ion-dipole, and H-bonding interactions of the DPPC ester moiety (cf. Table S2, SI).

A Computational Perspective for DPPC-Tryptophan Interaction. In order to obtain a closer look at the interfacial interactions elucidated from FT-IRRAS spectroscopy, density functional computations for DPPC headgroup interaction with H₂O and tryptophan at the closest approach provided the geometry optimized 1:1 adducts in Figure 9, where H-bonding (PO₂⁻···⁺NH₃), cation-π ((CH₃)₃N⁺-π(indole)), and ester carbonyl-cation (⁺NH₃) interactions are evident. The ester carbonyls of the lipid and the water molecules around the lipid headgroup enable dipole-dipole interaction and allow H-bonding with the amino acid. In addition, electrostatic interactions prevailed between the positively charged amino acid side chains and the negatively charged lipid phosphate groups. The geometry optimized 1:1 DPPC/tryptophan and DPPC/H₂O conformers evidence the binding to be thermodynamically favorable which are well supported from FT-IRRAS results in the preceding sections. Model clusters of prototype surfactants with varied numbers of water molecules at the interface have been computed with ab initio and molecular mechanics methods,⁴⁹ revealing hydrophilic interaction between the polar surfactant head groups

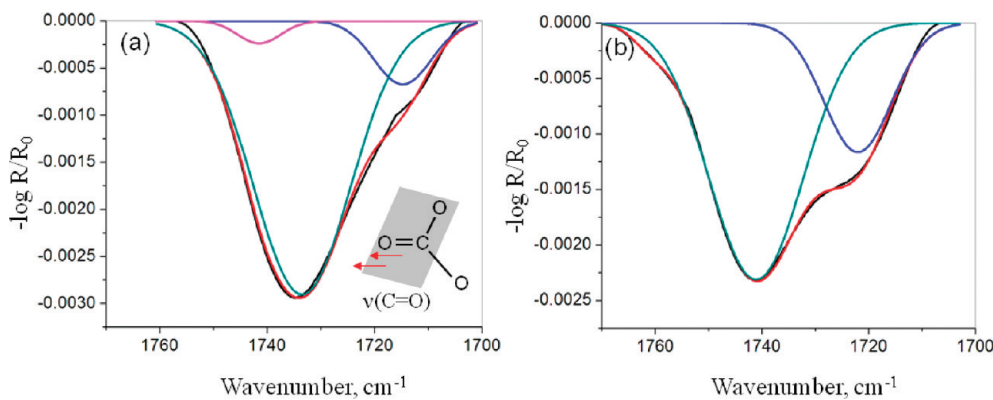


Figure 8. p-Polarized FT-IRRAS Gaussian deconvoluted spectra of the C=O stretching mode region of DPPC monolayers over (a) tryptophan and (b) water subphases at 40° angle of incidence at a surface pressure 40 mN/m.

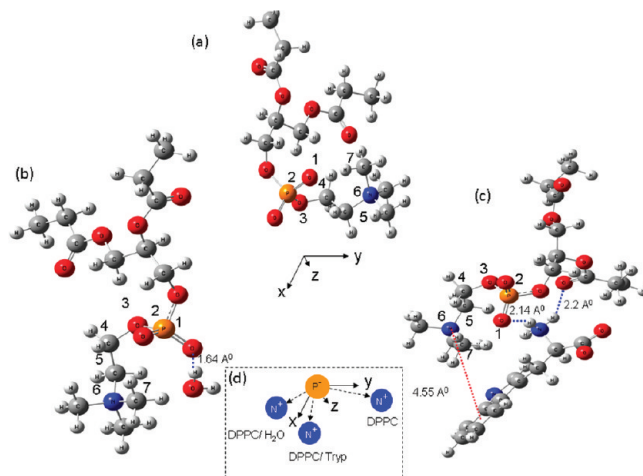


Figure 9. DFT (B3LYP/6-31G(d,p)) optimized (a) pure DPPC, (b) 1:1 adduct of DPPC/H₂O, and (c) 1:1 adduct of DPPC/trypotphan structures in vacuum showing characteristic molecular interactions. The PO₂⁻···H₂O H-bonding in (b) followed by (CH₃)₃N⁺–π (indole), PO₂⁻···NH₃⁺ H-bonding, and ester carbonyl–cation (+NH₃) interactions in a tryptophan environment in (c) are evident. For clarity, the C₁₆ chain is terminated at C1 (–CH₃) end group. N, O, and P atoms are shown in blue, red, and orange, respectively. (d) The varied orientation of the P⁻–N⁺ dipole of the DPPC headgroup for systems under study.

and the closest-contact water molecules. Insight on the active role of water as an interfacial monolayer counterpart and the surfactant behavior within the insoluble monolayer were the predominant findings.

Table 3 contains the optimized parameters of the 1:1 adducts showing drastic changes in their conformation with respect to the DPPC molecule alone; more specifically, the change of dihedral angle O₁P₂O₃C₄ from 6° in a pristine DPPC to 99° in DPPC: H₂O adduct has reoriented the P⁻–N⁺ dipole of the DPPC headgroup from a parallel orientation in the pure DPPC molecule to a vertical orientation at the interface with a reduction in the distance between the dipoles as a result of (PO₂⁻···HOH) hydrogen bonding. Similarly, for the DPPC/trypotphan adduct, the angular change from 6° to 38° justified a substantial reorientation of the dipole; an enhanced P⁻–N⁺ distance is indicative of the existing cation (choline)–π (indole) interaction, as substantiated from the FT-IRRAS features.

Estimation of Molecular Order: Orientation of Interfacial DPPC Monolayers. Molecular orientation in DPPC monolayers at 22 °C was quantitatively estimated from the magnitude of splitting of the methylene scissoring vibrational mode indicating a perpendicular orthorhombic structure^{50,51} (Figure 10). Here, the splitting is caused by intermolecular interaction between the adjacent molecules in the orthorhombic subcell.

Whereas the higher frequency component of the split orthorhombic CH₂ mode is polarized in the “a” direction of the subcell, the lower frequency component represents the part of the transition moment polarized along the “b” axis of the subcell, as shown in the inset. For polarized radiation, the integrated intensities of the two components are equal for a subcell orientation of 45°. Accordingly, orientation of the subcell in the XY plane could be evaluated from the component intensities of the split bands for the s- or p-polarized radiation. In Figure 10, the split methylene scissor bands of the DPPC monolayers from the tryptophan subphase are displayed for p- and s-polarization with intensities reversed for the 1465 and 1472 cm⁻¹ features implying orthogonality between the two molecules in the subcell. Thus, the orientation of the subcell in the XY plane was calculated on the basis of either p- or s-polarized measurements; the angle for the a direction of the subcell with the X axis as {arccot(I_p¹⁴⁷²/I_p¹⁴⁶⁵)} was estimated to be 37°. Although a decrease in the DPPC monolayer tilt angle from 30° in pure DPPC to almost 0° in a 1:1 molar ratio of DPPC and palmitic acid or 1-hexadecanol was reported,⁵² in the present work, an enhanced tilt from 26° over water to 37° over tryptophan subphase clearly evidenced reduced molecular order as a result of decreased attractive hydrophobic CH₂ chain interactions, induced by interfacial electrostatic and H-bonded interactions of the headgroup.

Tryptophan Modulated 2D DPPC Lattices: Influence of Temperature. For the saturated and symmetric dialkylphosphocholines, alkyl chain conformation inferred from the relative intensities of CH stretching vibrational bands depends on both alkyl chain length and interfacial concentration. Temperature-controlled experiments have shown lipid bilayer gel-to-liquid crystalline phase transition at 41 °C to play a pivotal role in determining the interfacial coverage and alkyl chain structure.⁵³ In spite of myriad reports on the 2D LE-LC phase transition of DPPC, a closer look at its in situ formed condensed phase 2D lattice characteristics influenced by several thermodynamic variables is clearly missing. The present investigation divulges important DPPC lattice structure and packing characteristics accrued from

Table 3. DFT/B3LYP 6-31G(d,p) Computed Structural Parameters for Pristine DPPC and Its H₂O and Tryptophan Adducts

system	P ⁻ –N ⁺ distance (Å)	$\angle O_3C_4C_5$ (deg)	$\angle C_4C_5N_6$ (deg)	dihedral angle (deg)		
				O ₁ P ₂ O ₃ C ₄	C ₄ C ₅ N ₆ C ₇	O ₃ C ₄ C ₅ N ₆
DPPC	4.266	111.31	113	6.02	64.76	-145.99
DPPC/H ₂ O (1:1)	4.040	111.72	117	99.27	-56.01	113.23
DPPC/tryptophan (1:1)	4.355	109.61	116	38.86	-57.79	134.53

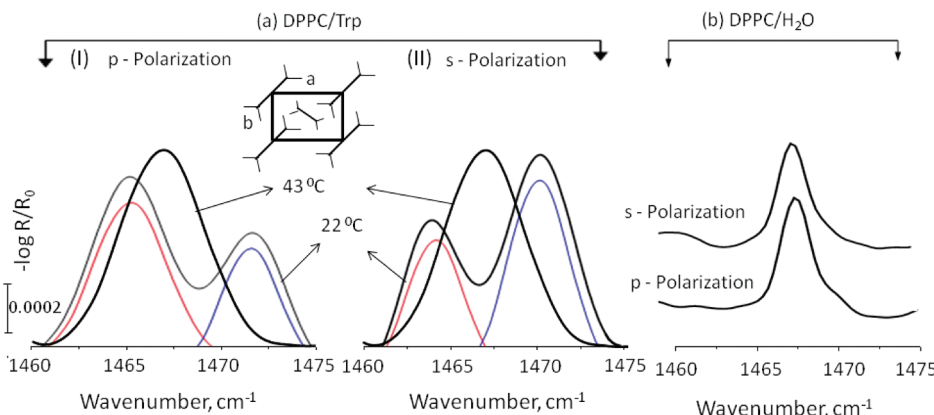


Figure 10. (a) Estimation of molecular tilt angle for DPPC monolayers on tryptophan subphase from the split methylene scissoring vibrational modes for (I) p- and (II) s-polarized IR beams at a surface pressure 40 mN/m at 22 °C and angle of incidence 40°; the split band intensity ratios $I_p^{1465}/I_p^{1472} = 1.33$, and $I_s^{1465}/I_s^{1472} = 1.30$ are visualized. The 43 °C spectral profiles in both cases imply a nonorthorhombic unit cell without methylene scissor band splitting. (b) The figure depicts the nonsplit methylene scissor bands for the DPPC monolayers over water subphase.

its interfacial interactions with tryptophan as a function of temperature. The pressure-area isotherms of DPPC monolayers on aqueous tryptophan subphase are collected in Figure 11a. The interfacial pressure associated with the LE-LC phase transition rises with temperature showing a strong dependence on it; a deduced transition temperature ~ 28 °C in the inset implies the surface pressure to irreversibly reach the terminal point for the LE-LC phase of DPPC monolayers at physiological tryptophan concentrations of 1 and 5 wt %. The nominal temperature-induced monolayer area increase for the condensed phase, sustaining a stable high pressure in Figure 11, panels a and b, indicates a reduction in free energy and hence a large barrier for the phosphocholine desorption from the interface. In addition, the 43 °C temperature treatment being beyond the DPPC's bulk phase LC to gel transition ($T_c = 41$ °C), a probable monolayer–vesicle fusion is evidenced from the small but finite increase in the molecular area of the condensed phase of DPPC at 40 mN/m. Tryptophan content in the monolayer was ruled out at all temperatures from the absence of free $\nu(NH)$ bands between 3460 and 3600 cm⁻¹ and the hydrogen bonded trans-NH bands with $\nu(NH)$ at 3320–3270 cm⁻¹, Figure 11c.⁵⁴ Intermolecular forces at the interface control the interfacial concentration and packing of the adsorbed DPPC, thus establishing changes in the 2D lattice structure. Accordingly, an in situ DPPC hexagonal subcell at 43 °C from a room temperature orthorhombic lattice packing was visualized in the present experiments. Order-disorder phase transitions of LB films of amphiphiles with amines and amide units have been reported at temperatures as high as 122 °C owing to intermolecular H-bonding interactions in comparison to free amides.⁵⁵

In Figure 11c, the $\delta(CH_2)$ mode splits into two bands centered at 1772 and 1465 cm⁻¹ at 22 °C, indicative of an orthorhombic unit cell containing two crystallographically alkyl independent

hydrocarbon chains.⁵⁶ On decreasing the temperature to 20 °C, the $\delta(CH_2)$ mode gives a singlet band at 1467 cm⁻¹, implying a hexagonal arrangement. At 24 °C, reappearance of the singlet is observed near 1468 cm⁻¹, confirming the transition to be in equilibrium with a hexagonal–orthorhombic–hexagonal pattern. On further increase of temperature to 26–28 °C, the band shifts to a higher wavenumber 1471 cm⁻¹ with band broadening, implying the transition to be associated with a triclinic packing.⁵⁷ With further increase in temperature to 43 °C, reappearance of the singlet at 1468.3 cm⁻¹ confirms a high temperature hexagonal packing symmetry, arrived via a triclinic arrangement.⁵⁸ The diverse crystalline structures of the aliphatic chains thus dictate the configuration of the membrane lipid. Of the four types of two-dimensional lattices—square, rectangular, oblique, and hexagonal—hydrocarbon chains have packed in all, except in the square lattice. Oblique and rectangular 2D lattices have implied specific chain packing in triclinic and orthorhombic 3D lattice subcells, respectively.⁵⁹ The ultimate packing however has been found to be a strong function of the lipid type, the method of crystallization, temperature, and pressure. With an increase in temperature of the tryptophan subphase above room temperature (22 °C), the area per molecule in Figure 11a increased, maintaining an almost constant collapse pressure. Temperature induced optimal chain packing commensurate with chain orientation. A hexagonal unit cell at 20 °C, complying with the spectral features in Figure 11d, implied loose chain packing, where the specific chain–chain interaction was reduced as a result of partial local rotations along the chain, yielding more gauche conformers at a lower temperature. The triclinic subcell indicative of the singlet $\delta(CH_2)$ feature at 1471 cm⁻¹ at 28 °C implied the adjacent CCC planes to be packed in a parallel fashion. Although the 2D pressure yielded a hexagonal phase at the lowest

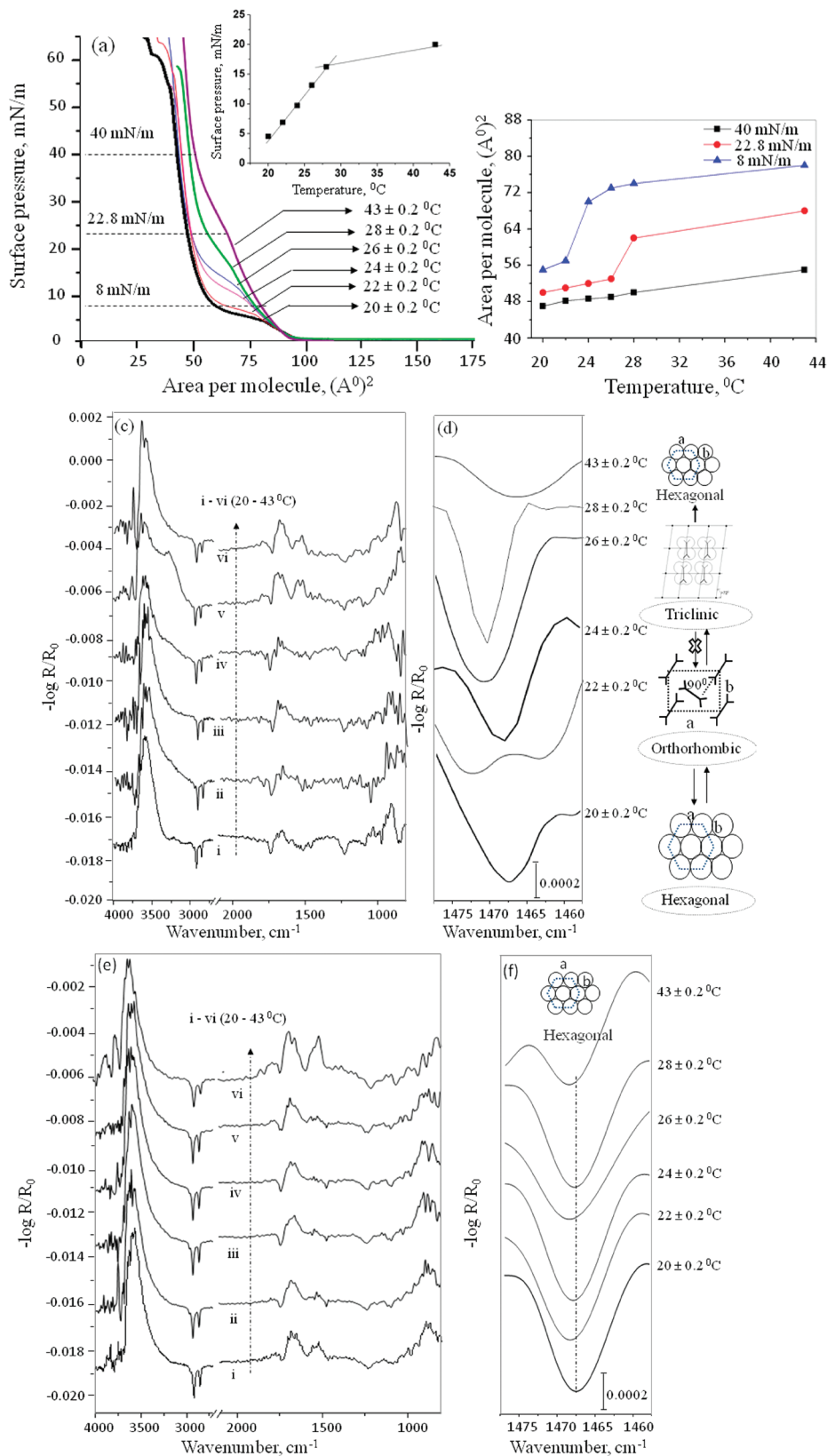


Figure 11. (a) Pressure-area isotherms of DPPC monolayers on aqueous tryptophan subphase (0.01 mg/mL, 1 wt %) in a temperature range between 20 and 43 °C. Inset shows variation of surface pressure for the LE-LC phase transition with temperature for 1 wt % tryptophan. Panel b shows the corresponding area vs temperature curves for three different phases at surface pressures 8, 22.8, and 40 mN/m. Panels c and e represent temperature dependent p-polarized FT-IRRAS spectra of DPPC monolayers on the aqueous tryptophan and water subphases at 40 mN/m, respectively. Panels d and f show the expanded regions of $\delta(\text{CH}_2)$ scissoring vibration for DPPC monolayers over tryptophan and water subphases respectively, along with their lattice packing. The spectra were acquired at 40° angle of incidence.

experimental temperature of 20 °C, which otherwise has been reported at higher temperatures,⁶⁰ experiments at 43 °C brought back the hexagonal unit cell, evidenced from the $\delta(\text{CH}_2)$ feature at 1473 cm⁻¹. The high temperature recurrence of hexagonal packing is indicative of a mixed DPPC monolayer with its vesicles upon vesicle fusion, evidenced from monolayer area increase (cf. Figure 11b), and that the molecular transfer from vesicle to monolayer was strongly influenced by temperature and surface charge.

Although the higher 5 wt % tryptophan subphase concentration repeated a similar order in the lattice structure/packing (Figure S4, SI), the DPPC/H₂O system as a function of temperature in Figure 11, panels e and f, showed only a hexagonal subshell throughout. The observations thus sufficed not only temperature but also the crucial role of the subphase tryptophan in governing the 2D DPPC lattice ordering influenced by lipid headgroup reorientation with changes in its angular distribution. The temperature dependent DPPC lattice subcells are thus a repercussion of competitive, attractive hydrophobic and repulsive steric interactions of the aliphatic chains and the electrostatics associated with the bulky choline headgroup at the interface in contact with tryptophan. Interaction of zwitterionic tryptophan with the DPPC monolayer induced a local surface reorganization of the underlying phospholipid molecules, triggered by favorable electrostatic interactions. The observed transitions between the two 2D crystalline states could be ascribed to weak first order transitions.

A temperature dependent crystal lattice transition has been reported for the crystal lattice of arachidic acid monolayer on a CdCl₂ subphase; a hexagonal packing of the hydrocarbon chains in the temperature range 293–283 K and at pH 6.2 transformed to an orthorhombic arrangement upon cooling at 283–280 K.^{61,62} Cadmium stearate monolayers have witnessed monotonic hexagonal subcells in a similar temperature duration. Addition of palmitic acid and 1-hexadecanol to DPPC in 1:1 molar ratio has strongly affected the phase transition temperature and molecular packing in DPPC monolayers; a change from a 30° tilt to an untilted molecular packing, with a significantly larger correlation length indicated a better ordered monolayer with elimination of the liquid-expanded to condensed phase transition at 30 °C.⁴⁰ Structural changes in a DPPC phospholipid bilayer induced by an external isotropic surface pressure in a range from 0.1 to 40 mN/m were computer simulated.⁶³ Molecular dynamics simulations showed that low pressures of ~0.1 to 1 mN/m did not affect the lipid structure or hydration of the lipid bilayer.

CONCLUSIONS

In understanding specific membrane functions, physicochemical properties of biological membranes are of critical importance. The main objective of this investigation was to establish the molecular interactions behind the preference of tryptophan for the DPPC membrane interface and to unravel the resulting 2D DPPC lattice structure as a function of temperature. Consequently, insight into the interaction between tryptophan and the DPPC lipid monolayer was obtained adopting highly sensitive, real time polarized FT-IRRAS spectroscopy in conjunction with DFT studies. The interaction of tryptophan with the polar headgroup of DPPC bound the phospholipid, modifying the network of hydrogen bonds with the tryptophan moiety, rather than with water. The interfacial DPPC monolayers witnessed a reoriented P⁻–N⁺ dipole of the DPPC headgroup

from a parallel orientation in the pure DPPC molecule to an almost vertical orientation at the interface. To sum up, the in-plane molecular organization probed by real time angle dependent polarized FT-IRRAS spectroscopy established an explicit relationship between the subphase dependent interface configuration and alkyl chain conformation within the monolayer that ultimately translated into varied subcell packing as a function of temperature. Pressure–area isotherms and the spectral results revealed the 2D lattice structure of the condensed phase domains to be strongly influenced by the subphase tryptophan and temperature with an interesting reversible/irreversible phase transition: a hexagonal-to-orthorhombic-to-triclinic-to-hexagonal pattern was observed over a wide temperature range of 20–43 °C and at a physiological pH, over a physiologically relevant tryptophan concentration. The study addressed the crucial role of tryptophan in the phase characteristics of DPPC monolayers mimicking a lipid–protein complex environment and resulted in monolayers that could serve as better models for the solid phase fraction of the lung surfactant monolayers at low protein/trypophan concentration. In addition, the temperature dependent 2D lattice transitions have provided quantum information on molecule transfer and the impact of a temperature pulse in a membrane environment, furnishing a model system to study intermembrane interactions. The alveolar air–water interfacial structures associated with the pulmonary surfactant in cellular environments would be better understood when under a thermal impact.

ASSOCIATED CONTENT

S Supporting Information. B3LYP/6-31G (d, p) level DFT energy minimized structures of DPPC and L-tryptophan, variation of s- and p-polarized $\nu_{\text{as}}(\text{CH}_2)/\nu_{\text{as}}(\text{CH}_2)$ ratios of antisymmetric and symmetric methylene bands as a function of angle of incidence at 22 °C and at higher temperatures, tabular data for Gaussian deconvoluted band assignments for DPPC monolayers on water and tryptophan subphases. This material is available free of charge via the Internet at <http://pubs.acs.org>.

AUTHOR INFORMATION

Corresponding Author

*E-mail: archita59@yahoo.com. Phone: 0091-44-2257-4217. Fax: 0091-44-2257-4202.

ACKNOWLEDGMENT

The authors thank the Department of Science and Technology, New Delhi, India for the financial support (Grant No. SR/S2/CMP-57/2006). N.K.S. acknowledges the Senior Research Fellowship from IIT Madras.

REFERENCES

- (1) Doyle, A. W.; Fick, J.; Himmelhaus, M.; Eck, W.; Graziani, I.; Prudovsky, I.; Grunze, M.; Maciag, T.; Neivandt, D. *J. Langmuir* **2004**, *20*, 8961–8965.
- (2) Jing, W.; Hunter, H. N.; Hagel, J.; Vogel, H. *J. J. Peptide Res.* **2003**, *61*, 219–229.
- (3) Bachar, M.; Becker, O. M. *Biophys. J.* **2000**, *78*, 1359–1375.
- (4) Hu, W.; Lee, K.-C.; Cross, T. A. *Biochemistry* **1993**, *32*, 7035–7047.
- (5) Jacobs, R. E.; White, S. H. *Biochemistry* **1989**, *28*, 3421–3437.
- (6) Chattopadhyay, A.; McNamee, M. G. *Biochemistry* **1991**, *30*, 7159–7164.

- (7) Schiffer, M.; Chang, C. -H.; Stevens, F. J. *Protein Eng.* **1992**, *5*, 213–214.
- (8) Zheng, H.; Du, X. *J. Phys. Chem. B* **2010**, *114*, 577–584.
- (9) Arouri, A.; Kerth, A.; Dathe, M.; Blume, A. *Langmuir* **2011**, *27*, 2811–2818.
- (10) Dyck, M.; Kerth, A.; Blume, A.; Lösche, M. *J. Phys. Chem. B* **2006**, *110*, 22152–22159.
- (11) Brauner, J. W.; Flach, C. R.; Xu, Z.; Bi, X.; Lewis, R. N. A. H.; McElhaney, R. N.; Gericke, A.; Mendelsohn, R. *J. Phys. Chem. B* **2003**, *107*, 7202–7211.
- (12) Wang, C.; Zheng, J., Jr.; Oliveira, O. N.; Leblanc, R. M. *J. Phys. Chem. C* **2007**, *111*, 7826–7833.
- (13) Dluhy, R. A. *J. Phys. Chem.* **1986**, *90*, 1373–1379.
- (14) Fina, L. J.; Tung, Y. S. *Appl. Spectrosc.* **1991**, *45*, 986–992.
- (15) Gericke, A.; Michailov, A. V.; Huhnerfuss, H. *Vib. Spectrosc.* **1993**, *4*, 335–348.
- (16) Tung, Y. S.; Gao, T.; Rosen, M. J.; Valentini, J. E.; Fina, L. *J. Appl. Spectrosc.* **1993**, *47*, 1643–1650.
- (17) Ren, Y.; Meuse, C. W.; Hsu, S. L.; Stidham, H. D. *J. Phys. Chem.* **1994**, *98*, 8424–8430.
- (18) Blaudez, D.; Turlet, J.-M.; Dufourcq, J.; Bard, D.; Buffeteau, T.; Desbat, B. *J. Chem. Soc., Faraday Trans.* **1996**, *92*, 525–530.
- (19) Möhwald, A. *Annu. Rev. Phys. Chem.* **1990**, *41*, 441–476.
- (20) Knobler, C. M. *Adv. Chem. Phys.* **1990**, *77*, 397–449.
- (21) Mao, G.; Desai, J.; Flach, C. R.; Mendelsohn, R. *Langmuir* **2008**, *24*, 2025–2034.
- (22) Vaknin, D.; Kjaer, K.; Nielsen, J. A.; Lösche, M. *Biophys. J.* **1991**, *59*, 1325–1332.
- (23) Brezesinski, G.; Dietrich, A.; Struth, B.; Böhm, C.; Bouwman, W. G.; Kjaer, K.; Möhwald, H. *Chem. Phys. Lipids* **1995**, *76*, 145–157.
- (24) Baltes, H.; Schwendler, M.; Helm, C. A.; Möhwald, H. *J. Colloid Interface Sci.* **1996**, *178*, 135–143.
- (25) Hosoi, K.; Ishikawa, T.; Tomioka, A.; Miyano, K. *Jpn. J. Appl. Phys.* **1993**, *32*, 135–137.
- (26) Weidemann, G.; Vollhardt, D. *Thin Solid Films* **1995**, *264*, 94–103.
- (27) Albrecht, O.; Gruler, H.; Sackmann, E. *J. Phys.* **1978**, *39*, 301–313.
- (28) Kewalramani, S.; Hlaing, H.; Ocko, B. M.; Kuzmenko, I.; Fukuto, M. *J. Phys. Chem. Lett.* **2010**, *1*, 489–495.
- (29) Grillo, D.; de la Cruz, M. O.; Szleifer, I. *Soft Matter* **2011**, *7*, 4672–4679.
- (30) Gzyl-Malcher, B.; Filek, M.; Brezesinski, G. *Langmuir* **2011**, *27*, 10886–10893.
- (31) Schleh, C.; Mühlfeld, C.; Pulskamp, K.; Schmiedl, A.; Nassimi, M.; Lauenstein, H. D.; Braun, A.; Krug, N.; Erpenbeck, V. J.; Hohlfeld, J. M. *Respir. Res.* **2009**, *10*:90.
- (32) Frisch, M. J.; Trucks, G. W.; Schlegel, H. B.; Scuseria, G. E.; Robb, M. A.; Cheeseman, J. R.; Montgomery, J. A. Jr.; Vreven, T.; Kudin, K. N.; Burant, J. C.; Millam, J. M.; Iyengar, S. S.; Tomasi, J.; Barone, V.; Mennucci, B.; Cossi, M.; Scalmani, G.; Rega, N.; Petersson, G. A.; Nakatsuji, H.; Hada, M.; Ehara, M.; Toyota, K.; Fukuda, R.; Hasegawa, J.; Ishida, M.; Nakajima, T.; Honda, Y.; Kitao, O.; Nakai, H.; Klene, M.; Li, X.; Knox, J. E.; Hratchian, H. P.; Cross, J. B.; Adamo, C.; Jaramillo, J.; Gomperts, R.; Stratmann, R. E.; Yazyev, O.; Austin, A. J.; Cammi, R.; Pomelli, C.; Ochterski, J. W.; Ayala, P. Y.; Morokuma, K.; Voth, G. A.; Salvador, P.; Dannenberg, J. J.; Zakrzewski, V. G.; Dapprich, S.; Daniels, A. D.; Strain, M. C.; Farkas, O.; Malick, D. K.; Rabuck, A. D.; Raghavachari, K.; Foresman, J. B.; Ortiz, J. V.; Cui, Q.; Baboul, A. G.; Clifford, S.; Cioslowski, J.; Stefanov, B. B.; Liu, G.; Liashenko, A.; Piskorz, P.; Komaromi, I.; Martin, R. L.; Fox, D. J.; Keith, T.; Al-Laham, M. A.; Peng, C. Y.; Nanayakkara, A.; Challacombe, M.; Gill, P. M. W.; Johnson, B.; Chen, W.; Wong, M. W.; Gonzalez, C.; Pople, J. A. *Gaussian 03*, revision B.04; Gaussian, Inc.: Pittsburgh, PA, 2003.
- (33) Kim, K.; Choi, S. Q.; Zasadzinski, J. A.; Squires, T. M. *Soft Matter* **2011**, *7*, 7782–7789.
- (34) Biji, P.; Sarangi, N. K.; Patnaik, A. *Langmuir* **2010**, *26*, 14047–14057.
- (35) Mark, P.; Nilsson, L. *J. Phys. Chem. B* **2002**, *106*, 9440–9445.
- (36) Mitchell, M. L.; Dluhy, R. A. *J. Am. Chem. Soc.* **1988**, *110*, 712–718.
- (37) Liao, K.; Du, X. *J. Phys. Chem. B* **2009**, *113*, 1396–1403.
- (38) Walker, R. A.; Conboy, J. C.; Richmond, G. L. *Langmuir* **1997**, *13*, 3070–3073.
- (39) MacPhail, R. A.; Strauss, H. L.; Synder, R. G.; Elliger, C. A. *J. Phys. Chem.* **1984**, *88*, 334–341.
- (40) Fringeli, P. U. Z. *Naturforsch.* **1977**, *32c*, 20–45.
- (41) Berkowitz, M. L.; Bostick, D. L.; Pandit, S. *Chem. Rev.* **2006**, *106*, 1527–1539.
- (42) Akutsu, H. *Biochemistry* **1981**, *20*, 7359–7366.
- (43) Shimanouchi, T.; Tsuboi, M.; Kyogoko, Y. *Infrared Spectra of Nucleic Acids and Related Compounds*; Wiley Interscience: New York, 1964; Vol. 7, pp 467–499.
- (44) Kooijman, E. E.; Burger, K. N. *J. Biophys. Acta* **2009**, *1791*, 881–888.
- (45) Zawisza, I.; Wittstock, G.; Boukherroub, R.; Szunerits, S. *Langmuir* **2008**, *24*, 3922–3923.
- (46) Ou-Yang, W.; Weis, M.; Manaka, T.; Iwamoto, M. *J. Chem. Phys.* **2011**, *134* (154709), 1–8.
- (47) Ma, G.; Allen, H. C. *Langmuir* **2006**, *22*, 5341–5349.
- (48) Popova, A. V.; Hincha, D. K. *Biophys. J.* **2003**, *85*, 1682–1690.
- (49) Ivanova, A.; Tadjer, A.; Tyutulkov, N.; Radoev, B. *J. Phys. Chem. A* **2005**, *109*, 1692–1702.
- (50) Flach, C. R.; Gericke, A.; Mendelsohn, R. *J. Phys. Chem. B* **1997**, *101*, 58–65.
- (51) Bihani, T. L.; Pézolet, M. *Chem. Phys. Lipids* **1998**, *94*, 13–33.
- (52) Lee, K. Y. C.; Gopal, A.; Nahmen, A.; Zasadzinski, J. A.; Majewski, J.; Smith, G. S.; Howes, P. B.; Kjaer, K. *J. Chem. Phys.* **2002**, *116*, 774–783.
- (53) Watry, M. R.; Tarbuck, T. L.; Richmond, G. L. *J. Phys. Chem. B* **2003**, *107*, 512–518.
- (54) Andreeva, T. D.; Petrov, J. G.; Brezesinski, G.; Möhwald, H. *Langmuir* **2008**, *24*, 8001–8007.
- (55) Du, X.; Liang, Y. *J. Phys. Chem. B* **2000**, *104*, 10047–10052.
- (56) Snyder, R. G. *J. Mol. Spectrosc.* **1961**, *7*, 116–144.
- (57) Du, X.; Miao, W.; Liang, Y. *J. Phys. Chem. B* **2005**, *109*, 7428–7434.
- (58) Holland, R. F.; Nielsen, J. R. *J. Mol. Spectrosc.* **1962**, *9*, 436–460.
- (59) Small, D. M. *J. Lipid Res.* **1984**, *25*, 1490–1500.
- (60) Müller, A. *Proc. R. Soc. London Ser. A* **1932**, *138*, 514–530.
- (61) Ren, Y.; Limura, K.; Kato, T. *J. Chem. Phys.* **2001**, *114*, 1949–1951.
- (62) Ren, Y.; Hossain, Md. M.; Limura, K.; Kato, T. *Chem. Phys. Lett.* **2000**, *325*, 503–507.
- (63) Cascales, J. J. L.; Otero, T. F.; Romero, A. J. F.; Camacho, L. *Langmuir* **2006**, *22*, 5818–5824.